M. Del Soldato · A. Riquelme · S. Bianchini · R. Tomàs · D. Di Martire · P. De Vita · S. Moretti · D. Calcaterra

# Multisource data integration to investigate one century of evolution for the Agnone landslide (Molise, southern Italy)

**Abstract** Landslides are one of the most relevant geohazards worldwide, causing direct and indirect costs and fatalities. Italy is one of the countries most affected by mass movements, and the Molise region, southern Italy, is known to be susceptible to erosional processes and landslides. In January 2003, a landslide in the municipality of Agnone, in the Colle Lapponi-Piano Ovetta (CL-PO) territory, occurred causing substantial damage to both structures and civil infrastructure. To investigate the evolution of the landslide-affected catchment over approximately one century, different data were taken into account: (i) literature information at the beginning of the twentieth century; (ii) historical sets of aerial optical photographs to analyse the geomorphological evolution from 1945 to 2003; (iii) SAR (Synthetic Aperture Radar) data from the ERS1/2, ENVISAT and COSMO-SkyMed satellites to monitor the displacement from 1992 to 2015; (iv) traditional measurements carried out through geological and geomorphological surveys, inclinometers and GPS campaigns to characterize the geological setting of the area; and (v) recent optical photographs of the catchment area to determine the enlargement of the landslide. Using the structure from motion technique, a 3D reconstruction of each set of historical aerial photographs was made to investigate the geomorphological evolution and to trace the boundary of the mass movements. As a result, the combination of multitemporal and multitechnique analysis of the evolution of the CL-PO landslide enabled an assessment of the landslide expansion, which resulted in a maximum length of up to approximately 1500 m. A complete investigation of the past and present deformational sequences of the area was performed to potentially plan further mitigation and prevention strategies to avoid possible reactivations.

## Introduction

Landslides are one of the most important and widespread natural hazards affecting the Italian territory (Herrera et al. 2018), partially due to climate change with serious effects on the environment and geomorphology (Crozier 2010). This affirmation is supported by several data sets showing the events and people involved in landslide occurrences as well as the economic and social consequences and the damage to structures and infrastructure (Schuster and Highland 2001; Kjekstad and Highland 2009; Del Soldato et al. 2017). The Italian Landslides Database includes up to 528.903 landslides in Italy, which is the European country with the highest density of landslides (the landslide area represents 7.3% of the territory) (Herrera et al. 2018). Since the beginning of the twentieth century, more than 1400 landslides occurred at approximately 1200 different sites in Italy (Salvati et al. 2015). This suggests that several mass movements are reactivations in previously affected areas. Landslide evolution in different environments plays a key role in investigating possible

future urban development (e.g. Van Westen and Lulie Getahun 2003; Korup et al. 2010; Giordan et al. 2013). Studies of landslide evolution that improve the knowledge of ground movements are essential to understand the mechanism of deformation (Casson et al. 2003) for landslide-prone territories to mitigate the associated risk and to prevent landslide occurrences or reactivations.

Remote sensing techniques such as persistent scatterer interferometry (PSI) data (e.g. Massonnet and Feigl 1998; Ferretti et al. 2001; Farina et al. 2006; Hooper et al. 2012) and change detection methodologies (e.g. White 1991; Ferretti et al. 2001; Lu et al. 2004; Dekker 2005; Farina et al. 2006) have been successfully exploited to detect and map slow-moving landslides at a local or regional scale to perform back-analysis to better define boundaries and ground rates of movements, as well as to identify the most critical landslide-affected sites over wide areas (Solari et al., 2018). Although they are powerful instruments to investigate, map and monitor natural processes, satellite optical and radar images have been available for approximately the last 25 years. A breakthrough in the study of the evolution of natural processes was to use different techniques to investigate the longest possible period (e.g. by means of new tools to analyse historical aerial photographs), which enabled an analysis of approximately the last 70 years (e.g. Van Westen and Lulie Getahun 2003). In the late 1970s, Ullman (1979) developed the structure from motion (SfM) technique that was only recently applied to geomorphological studies of the evolution of the Earth's surface, taking advantage of similar tenets from stereophotogrammetry (Snavely et al. 2008; Westoby et al. 2012; Eltner et al. 2016). This approach enables the reconstruction of 3D models of various surfaces by overlapping several digital photos. Some common applications of SfM in the literature include 3D reconstruction of external façades of buildings and monuments (e.g. Snavely et al. 2008; Furukawa and Ponce 2010), archaeological sites (e.g. Doneus et al. 2011; Verhoeven 2011; Verhoeven et al. 2012), generation of digital elevation models (DEM) by means of Unmanned Aerial Vehicles (UAV) (e.g. Turner et al. 2012; Lucieer et al. 2013; James and Robson 2014), change detection (e.g. Abellán et al. 2009) and rock mass characterization (Sturzenegger et al. 2011; Riquelme et al. 2014).

The regions in southern Italy involved in the geologically recent Apennines mountain chain are highly susceptible to landslides (Cotecchia and Melidoro 1974) due to the complex geological setting, characterized by several different structurally convoluted lithologies (Esu 1977). More than 4000 mass movements (Rosskopf and Aucelli 2007) and incipient erosional processes (Marchetti 2016) are known to affect the territory of the Molise region despite its limited area.

The aim of this work is an analysis of the evolution of the landslide that occurred in the Colle Lapponi-Piano Ovetta catchment (CL-PO), in the municipality of Agnone (Molise, southern Italy), by combining different remote sensing techniques, e.g.

SfM and InSAR, and field surveys, i.e. geomorphological investigations and in situ data, i.e. GPS and inclinometer measurements. This process will be supported by historical literature information and geomorphological and topographical data in order to determine the geomorphological evolution over approximately one century of the CL-PO landslide-prone area. To achieve this goal, different data were collected, e.g. historical optical photographs, ancillary and field data, and radar satellite images and products. Several 3D reconstructions of the CL-PO landslide were produced and analysed by using sets of historical aerial photographs captured in 1945, 1954, 1981, 1986, 1991 and 2003. Although historical aerial imagery has several limitations, e.g. a bi-dimensional vision of the territory in greyscale, they still play a fundamental role in the studies of environmental and landscape evolution (Carrara et al. 2003; Van Westen and Lulie Getahun 2003; Giordan et al. 2013). By analysing all the available data, approximately one century of evolution for the CL-PO landslide-prone area, from the beginning of the twentieth century to 2015, was investigated.

### Site description and available data

The municipality of Agnone is a Sannitic archaeology site located in the northern part of the Molise region (southern Italy), which has an area of approximately 96 km², and the territory is strongly affected by both landslides and erosional processes, as the major part of the Molise region. The historical town of Agnone is located at approximately 800 m a.s.l., and it is bathed by Verrino creek. The climate of the region is moderate, with alternating cold temperatures with rain and snow thundershowers during autumn-winter and arid periods during spring-summer. The investigated mass movement is a deep-seated large roto-translational slide resulting in earth flow in the lower portion, characterized by a complex movement (Calcaterra et al. 2008) affecting the western territory of the municipality in the catchment of the S. Nicola valley, tributary of the Verrino creek on the hydrographic right side.

Since the beginning of the twentieth century, the CL-PO catchment has been affected by the landslide. In March 1905, the bridge of the main access road to Agnone crossing the Verrino creek was damaged by a gravity phenomenon due to an intense rainfall period combined with snow-melting (Almagià 1910; Calcaterra et al. 2008). Successively, the Agnone municipality has been affected by several small and large landslide phenomena reported in the national AVI Project (Guzzetti et al. 1994), revealing more than 60 landslides in the territory between 1970 and 1998. Between January 23rd and 27th, 2003, an important remobilization involved a large area of the historically dormant CL-PO landslide, causing deformations over the whole basin and forcing the local authorities to adopt restrictive measures for 13 edifices occupied by 17 families located within and nearby the landslide. Furthermore, two country roads adjacent to the landslide remain closed due to the substantial damage caused by this event. The mass movement subsequently reactivated in 2004, 2005 and between 2006 and 2007, which induced the local administration to allocate resources for some urgent interventions to intercept superficial waters and drain a pond formed in the upper portion of the affected area, in addition to geomorphological reshaping work. Despite these strategies, the ground displacements increased, which caused the cracking and sliding of structures and of a road located uphill of the landslide. These damages were mapped and categorized by several damage classification approaches (Del Soldato et al. 2016a).

The CL-PO territory is geologically characterized by the Mount Pizzi-Agnone and Colle Albero-Tufillo units outcropping with the two members of Agnone Flysch and a lower marly formation (Fig. 1a). The members of the Agnone Flysch are catalogued as "*Structurally Complex Formations*", geological materials characterized by large and scale-dependent heterogeneity in lithological and structural features that suffered complex compressional and extensional geological phases (Esu 1977). The geotechnical parameters of these types of formations are influenced by heterogeneity as well as scaly fabric with the alternation of "hard" (rock-like material) and "weak" horizons (soil-like material) (Almagià 1910; Cotecchia and Melidoro 1974; Guida and Iaccarino 1991; Di Maio et al. 2010).

The lower member of the Agnone Flysch formation presents alternations of marl limestones, marls and calcarenites, in addition to deposits of silico-clastic turbidites composed of thin intercalations of clayey sandstones, sandstones and arenites. The upper member of the Agnone Flysch is constituted by an alternation of marly, semi-coherent clayey and subordinate greyish sandy layers with low mechanical resistance, diffuse alteration traces and lithoid sandstones or calcareous intercalations with highly variable thicknesses. Inside both members, some olistoliths of older conglomeratic material are recognizable (Vezzani et al. 2004; Filocamo et al. 2015). Furthermore, weathering effects caused discoloration, decomposition and weakening, forming a superficial regolith horizon featured by clays, silty clays and subordinate sand with diffuse alteration traces, abundant organic material and several clasts. A cross-section (A-A′) was traced along the CL-PO landslide area and is shown in Fig. 1b.

The geotechnical characterization of the area affected by the landslide has been made by the re-interpretation of two geological and geotechnical campaigns from 2004 to 2006. The latter consists of 39 boreholes with depths between 10.5 and 40.0 m that have allowed the identification of four homogeneous layers (Calcaterra et al. 2008) from bottom to top as follows:

> Level D—marly clays, marls and clayey marls with silty and clay fractions.
>
> Thickness: 15.30–20.00;
>
> Level C—calcareous layers with thickness up to several metres.
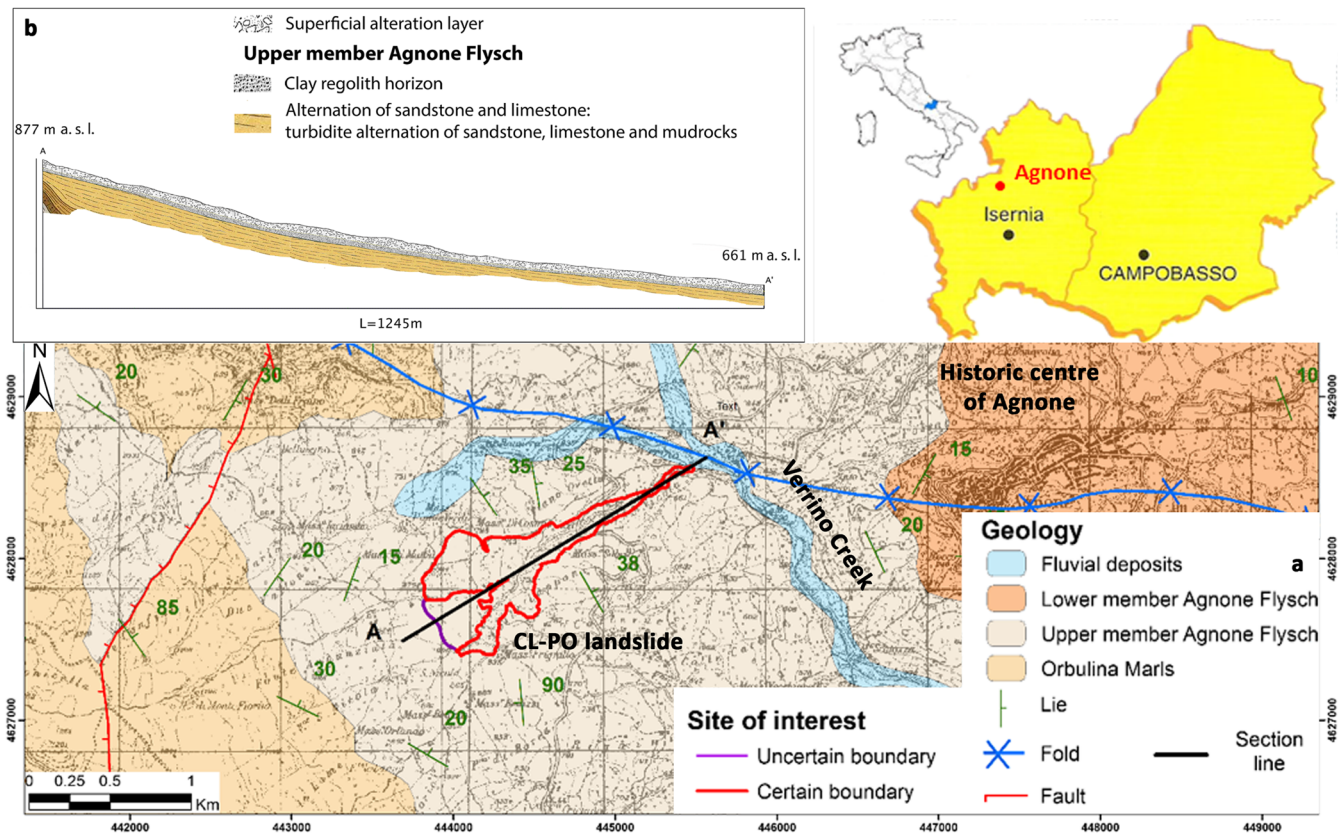>
> Thickness variable from dm to m;
>
> Level B—grey clays, silty clays, sandy clay and silty sands with a medium plasticity.
>
> Thickness: 4.00–12.00;
>
> Level A—chaotic and plastic matrix including dispersed fragments of resistant rock and mudstone.
>
> Thickness: 6.70–11.20.

**Fig. 1** **a** Localization and geological sketch map (Vezzani et al. 2004) of the area of interest in Agnone with the currently known contour of the landslide reported in red and the possible larger outline in purple. **b** Geological section A-A′ is traced along the area of interest of the CL-PO landslide (Vezzani et al. 2004)

The bottom level (i.e. Level D) was directly involved in the 2003 reactivation of the CL-PO landslide.

Furthermore, some inclinometers and piezometers were installed in the boreholes, but they recorded only for a short time due to the continued displacement that caused their failure.

Ancillary data (e.g. DEM and derived maps), information acquired by means of remote sensing techniques (i.e. historical optical aerial photos, radar satellite images and PSI), as well as direct investigations supported by instrumental monitoring, were used for the long-term investigation of the landslide. A DEM with a 5-m cell resolution was provided by the Molise region and useful information (e.g. aspect, which is a derived map showing the directional, with respect to the azimuth, exposures of the slopes of the area; and slope, which is a parameter indicating the inclination in degrees of the sides of the areas, with respect to the horizontal surface) was extrapolated by means of geographical tools in a geographical information system (GIS) environment to characterize the morphological parameters of the area and to better interpret the remote sensing data.

The landslide includes the territory from the Verrino creek at approximately 660 m a.s.l. up to 870 m a.s.l. and the morphology of the surrounding area strongly controlled by the slope parameters and the different local lithotypes. Where high topographical gradients are present, from 30° to 35°, the calcareous formations outcrop, while lower slope gradients, from 5° to 10°, correspond to areas

characterized by clayey Flysch units. Significant erosional processes affect regions with slope angle values greater than 15–20°.

The oldest available data used in this work are the historical aerial photographs captured by the Italian *Istituto Geografico Militare* (IGM) from 1942 to 2003. Starting from 1942, the IGM made recurring flights covering almost the entire Italian territory shooting greyscale nadir pictures with partial overlap. The first set of historical aerial photographs shot on the CL-PO landslide area was captured in 1945. This was followed by five additional flights recording a series of photographs over the area of interest dating back to 1954, 1981, 1986, 1991 and 2003 (Table 1).

Since 1992, the back investigation of the CL-PO landslide evolution is supported by information from SAR Interferometry (InSAR). ERS1/2 and ENVISAT data from 1992 to 2000 and from 2002 to 2010, respectively, are available through the PST-A (*Piano Straordinario di Telerilevamento Ambientale*) project and the Web Map Service (WMS) of the Italian Ministry for the Environment, Land and Sea. Furthermore, to cover the period of 2012–2015, 88 images acquired by COSMO-SkyMed constellations of the Italian Space Agency (ASI - *Agenzia Spaziale Itliana*) were collected in the framework of a specific project (Table 2) that allowed us to extend the investigated period. The ERS1/2 and ENVISAT data deriving from the *Portale Cartografico Nazionale* were elaborated by the PSInSAR technique (Persistent Scatterers Interferometry SAR) developed by TRE-ALTAMIRA (Ferretti et al. 2000, 2001). The COSMO-

**Table 1** Characteristics of the available historical aerial photographs used in this work

| Acquisition year | Number of photos | Estimated scale | Flying height (m) | Focal length (mm) |
|---|---|---|---|---|
| 1945 | 4 | 1:55000 | 7500 | 137 |
| 1954 | 8 | 1:33000 | 6000 | 153.01 |
| 1981 | 5 | 1:30000 | 5200 | 152.55 |
| 1986 | 4 | 1:28000 | 5100 | 152.55 |
| 1991 | 6 | 1:36000 | 6070 | 153.22 |
| 2003 | 4 | 1:35000 | 5300 | 153.31 |

SkyMed images were processed by the Coherence Pixel Technique (CPT) developed by the Remote Sensing Laboratory (RSLab) of the Universitat Politècnica de Catalunya, Spain (Mora et al. 2003; Blanco-Sanchez et al. 2008; Iglesias et al. 2015).

As the mobilized material and the widespread vegetation cover caused a low backscatter radar signal from the landslide body, in 2010, eight corner reflectors (CRs) were installed in the mass movement to enhance the signals reflected in the direction of the radar. The collected data were used to increase the knowledge about the displacement affecting the internal portion of the landslide (yellow triangles in Fig. 2). Although the corner reflectors were correctly positioned (four visible by the ascending orbit and four by the descending orbit), the high velocity of displacement affecting the area, some man-operated motions carried out by the land owners, damage or vegetation recovery made them invisible to the satellite analysing the entire dataset of CSK images. The corner reflectors were also used as benchmarks for differential GPS measurements during the campaigns developed since 2010. In addition, GPS measurements were collected for some benchmarks (green circles in Fig. 2) to investigate the displacements of the ground surface and increase the spatial point density throughout the entire landslide.

During the survey campaigns in 2006, five inclinometers were installed (orange circles in Fig. 2). Four of them were placed in the existing boreholes used for geotechnical investigations, while another one was placed out of the mobilized area to validate the displacement recorded by remote sensing techniques and to monitor the kinematic evolution of the landslide after the main reactivation. Relevant movements recorded along a sliding surface caused the failure of one of the inclinometers (S2), which was successively substituted (S5). Additionally, the inclinometer 2D measurements identified the depth of the rupture surface of the landslide and were used to control the efficiency of the adopted mitigation measures.

## Methodology

The assessment of the landslide evolution has been provided by a historical investigation of the literature and analyses conducted with traditional instruments, i.e. inclinometers and GPS campaigns, field surveys and remote sensing techniques. Six sets of historical aerial photographs were interpreted by means of 3D reconstruction of the landslide area obtained via the SfM technique (Ullman 1979) (Fig. 3). Hence, a qualitative comparison between historic and recent available data sets was possible. This analysis shows that several factors, such as the geometrical distortion of the photographs, the ortho-rectification stage and the physical condition of the aerial photos are to be considered in the interpretation.

Furthermore, GPS measurement campaigns, inclinometers and remote sensing techniques were applied to monitor the evolution of the CL-PO landslide since the main reactivation in January 2003 until 2015.

### 3D reconstruction of historical aerial photographs

The use of historical imagery allowed the recreation of a 3D image by means of a stereoscopic sight to detect, map and monitor unique geomorphological shapes across several decades (Hapke 2005).

**Table 2** Main features of the interferometric products dataset used to study the CL-PO landslide

| Features | ERS | ERS | ENVISAT | ENVISAT | CSK | CSK |
|---|---|---|---|---|---|---|
| Wavelength | C (~ 5.6 cm) | C (~ 5.6 cm) | C (~ 5.6 cm) | C (~ 5.6 cm) | X (~ 3.1 cm) | X (~ 3.1 cm) |
| Incidence angle, $\theta$ | ~ 23° | ~ 23° | ~ 23° | ~ 23° | 26.6° | 26.6° |
| Orbit | Ascending | Descending | Ascending | Descending | Ascending | Descending |
| Ground resolution, m (azimuth × range) | 4 × 20 | 4 × 20 | 4 × 20 | 4 × 20 | 3 × 3 | 3 × 3 |
| Revisit time (days) | 35 | 35 | 35 | 35 | 16 | 16 |
| Temporal span (day/month/year) | 25/04/1993 | 08/06/1992 | 29/11/2002 | 07/11/2002 | 15/10/2012 | 13/02/2012 |
| | 13/12/2000 | 07/12/2000 | 30/07/2010 | 03/06/2010 | 01/05/2015 | 15/01/2014 |
| Processing method | PSInSAR™ | PSInSAR™ | PSInSAR™ | PSInSAR™ | CPT | CPT |
| No. of images used | 54 | 78 | 50 | 45 | 41 | 47 |
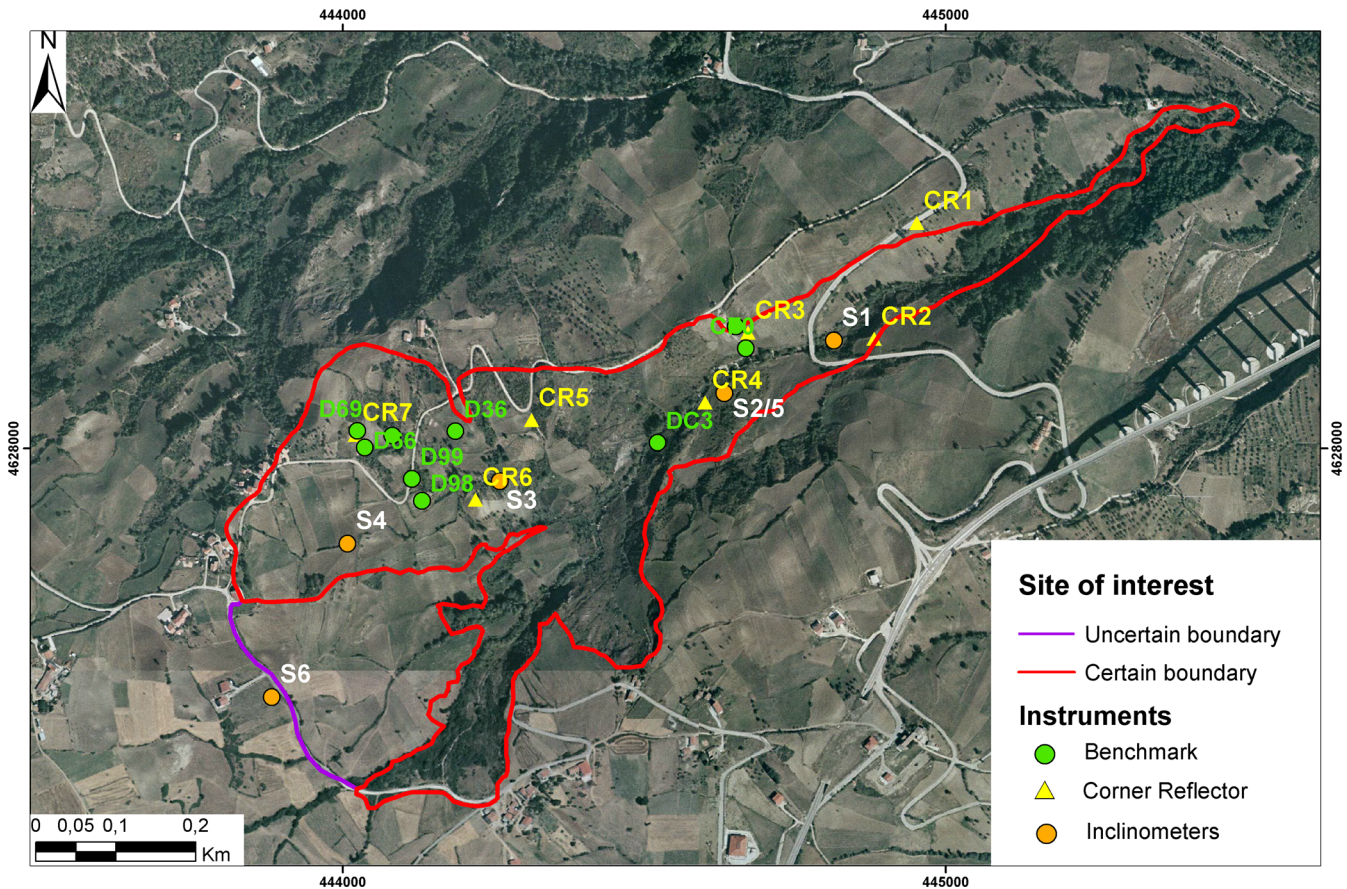
**Fig. 2** CL-PO landslide with the location of the benchmarks (green circles), the corner reflectors (yellow triangles) and the inclinometers (orange circles)

In this work, the SfM technique for digital photographs and algorithms optimized for the graphic processing unit (GPU) (Lucieer et al. 2013), implemented in the Agisoft Photoscan Professional edition software (Agisoft 2016), was applied to the historical aerial image analysis (Del Soldato et al., 2016b) after adapting some parameters. This software works with sets of digital photographs captured at the same time and partially overlapped (at least 60%, Agisoft 2016) covering the area of interest. By means of a redundant iterative bundle adjustment procedure, the SfM approach extracts information to solve the geometry of the scene, the camera parameters and the orientation for each set of photographs (Snavely et al. 2008), dramatically reducing the number of unknowns during the alignment procedure. The 3D Points Cloud (3DPC) represents the geometry/ structure of the scene that is generated by applying the SfM approach to the overlapped area between at least two images (Hartley and Zisserman 2003; Szeliski 2010; Fisher et al. 2013) in local coordinates. The input of several Ground Control Points (GCPs; points with known object-space coordinates in a system chosen by the operator) and Tie Points (points without coordinates; useful to better correlate the photographs and limit the distortion between them) allows georeferencing the 3DPC to a specific coordinate system. At the end, the obtained 3D reconstructions for all the available sets of photographs were extracted and imported in the environmental GIS with the collected

ancillary data and the calculated data for the CL-PO landslide. Hence, a better investigation of the interpretations of the area affected by the landslide through time could be conducted.

The analysis of the six available sets of photographs covering the CL-PO landslide-prone area can be subdivided into three main stages: (i) data preparation; (ii) data processing and 3D reconstruction; and (iii) extraction of the products and results. The application of the SfM approach on historical aerial photographs requires an adaption to the traditional workflow (Gomez et al. 2015; Ishiguro et al. 2016). The precision of the 3D reconstruction depends on several factors such as the grade of conservation of the photos, based on the scratches or markings on them, the scan resolution and the distortion introduced during this process, the overlap between adjacent photos and the identification, in addition to the input of GCPs and Tie Points.

Historical aerial photos used in this work were captured with non-digital cameras. Therefore, they were available in printed format and were scanned for the 3D reconstruction by the software. The information of the flight and the camera used for the acquisition of the photographs are reported in a black border around the pictures. During the preparation of the photographs for the software, these borders have to be carefully removed since they do not contain useful information for the 3D reconstructions. It is important to maintain the centre of the images and the
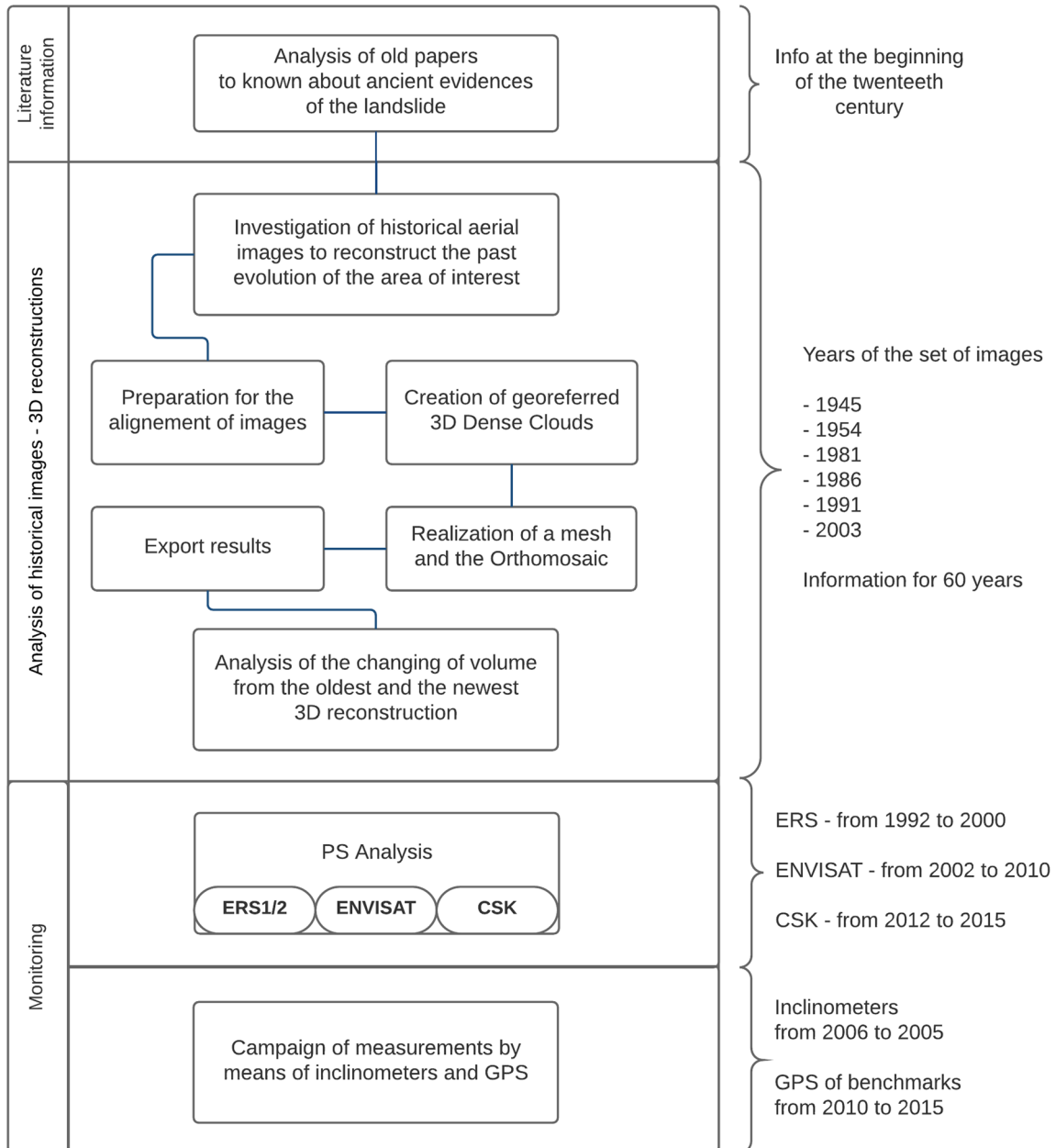
**Fig. 3** Schematic flowchart of the evolution investigation technique applied to the CL-PO landslide
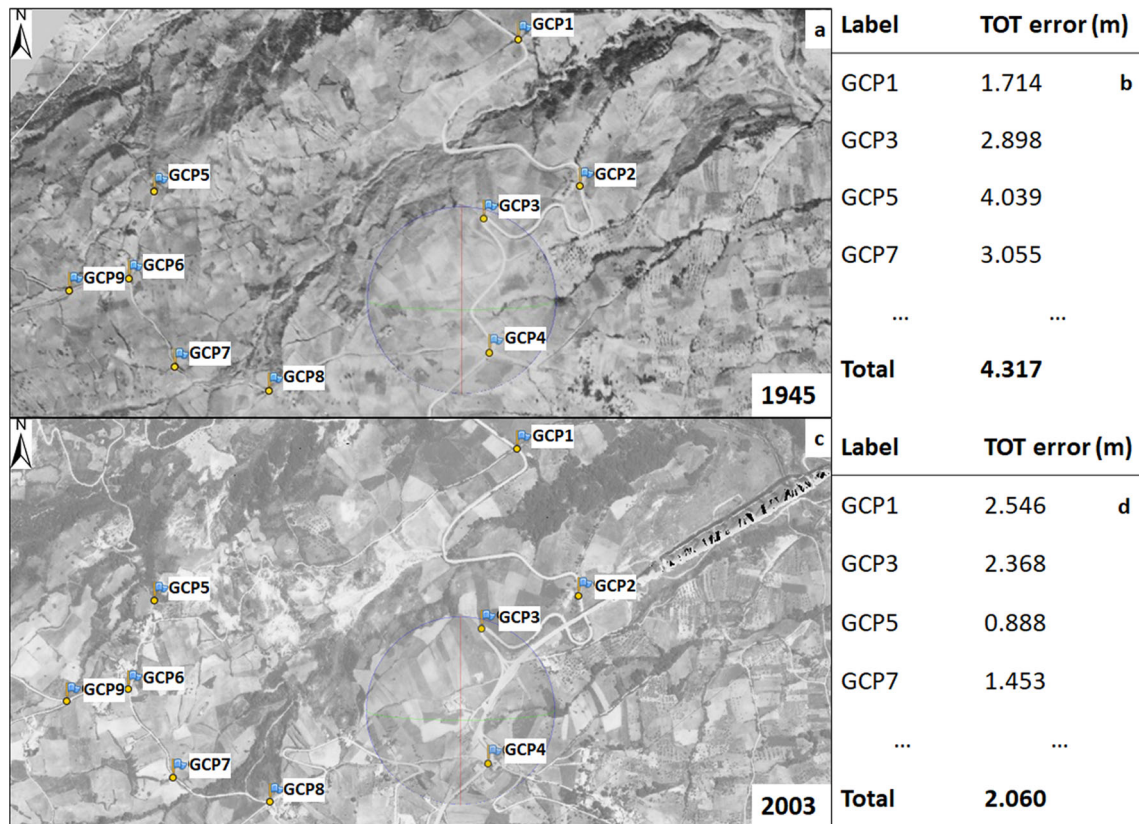
number of pixels when cropping the images. This allows the SfM software to recognize the set of photographs as captured by the same camera to apply the same camera calibration. Once the photographs were prepared, the cameras were aligned, and a sparse point cloud was generated. Subsequently, GCPs were inserted around the landslide to georeference the 3DPC and to correct non-linear deformations (Fig. 4a, c) on the mesh.

The input of GCPs is a very delicate task that has to be conducted with high accuracy by identifying some stable points from the oldest photographs to the newest ones, to obtain the greatest possible precision. For each inserted GCP, the errors in metres are presented (Fig. 4c, d). Since the coordinates of the GCPs were extracted from a DEM with a 5-m cell resolution, even

if the GCPs were added to historical aerial photographs scanned at a higher resolution, i.e. 600 dpi, the maximum resolution that could be attained was 5 m. The smaller values of precision resulting from the alignment and georeferencing process indicate that the algorithm optimized the results.

For each scenario, the number of inserted GCPs depends on the georeferencing precision; the aim was to reach a maximum total error of 5 m. In Table 3, the statistics of the errors derived from each set of photographs used for the 3D reconstructions are reported.

The last step enables the creation of the mesh to reproduce a georeferenced DEM and the orthomosaic images by means of dedicated tools in the PhotoScan Pro software. All the realized

| Label | TOT error (m) | |
|---|---|---|
| GCP1 | 1.714 | **b** |
| GCP3 | 2.898 | |
| GCP5 | 4.039 | |
| GCP7 | 3.055 | |
| ... | ... | |
| **Total** | **4.317** | |

| Label | TOT error (m) | |
|---|---|---|
| GCP1 | 2.546 | **d** |
| GCP3 | 2.368 | |
| GCP5 | 0.888 | |
| GCP7 | 1.453 | |
| ... | ... | |
| **Total** | **2.060** | |

**Fig. 4** Some GCPs on the oldest Dense Cloud of the scenario in 1945 (**a**) and in the newly reconstructed mesh of 2003 (**b**), with the respective accuracies of some sample GCPs (**c** and **d**, respectively)

products, i.e. 3DPC, the mesh of the georeferenced DEM and the orthomosaic can be extracted in several ways in order to be used by other scientific software for the interpretation.

The 3DPCs are mounted in the Cloud Compare software to better investigate and compare the resulting products by zooming and rotating them in a 3D view. In addition, the colour of each point reproduces the value, in RGB, of the source historical photographs. This allows better identification and localization of scarps, counterslopes and ground tension cracks by means of both visual investigation and recognizable geomorphological changes. The realized meshes and DEMs for all the sets of historical aerial photographs were added in a GIS environment to combine them with both sets of ancillary data. Hence, a better interpretation of the ground displacements of the catchment can be conducted in order to define a boundary around the area involved in the landslide.

### DInSAR technique

The analysed data were acquired by ERS1/2, ENVISAT and COSMO-SkyMed constellations from 1992 to 2015. ERS1/2 and ENVISAT data were processed by the PSP (Costantini et al. 2008) and PSInSAR technique developed by TRE-ALTAMIRA (Ferretti et al. 2000, 2001). COSMO-SkyMed images were processed by the *SUBSOFT processor* using the CPT algorithm developed by the Remote Sensing Laboratory (RSLab) of the Universitat Politècnica de Catalunya (Mora et al. 2003; Blanco-Sanchez et al. 2008). The

derived PS (Persistent Scatterer) data were classified using a colour scale indicated by hot colour displacement moving away from the sensor and cold colour data moving towards the satellite. The stability range ($\pm 1.5$ mm/year) is coloured in green, based on the standard deviation of the processed product.

Several studies demonstrated that the in-depth analysis of PS time series located at relevant sites can assist with the understanding of the dynamic and temporal evolution of ground motions for a slope (Meisina et al. 2008; Cigna et al. 2011; Confuorto et al. 2017). Notti et al. (2015) proposed a three-step procedure that does not interfere with InSAR processing to exploit the information derived from time series: (a) Pre-Processing evaluating the SAR Dataset Quality Index (SDQI); (b) Post-Processing, improving the quality of the previously processed time series data applying an empirical/stochastic method to remove single data anomalies as well as noise and regional trends; and c) detection and correction of possible phase unwrapping errors. The time series from the area of interest were subjected to a time series improvement in the Post-Processing phase (Notti et al. 2015) to remove anomalies from the regional trend. This type of effect or anomaly, not related to natural processes affecting the ground surfaces, can be easily detected since the entire dataset is affected. To identify the regional noise, data with high coherence (e.g. higher than 0.9) and an average LOS velocity between $- 0.5$ mm/year and $+ 0.5$ mm/year were selected and averaged. The average regional trend has to be subtracted from the original trend,

**Table 3** RMSE control points for each reconstructed set of historical aerial images

| Set of images (year) | Number of GCPs | Number of tie points | X error (m) | Y error (m) | Z error (m) | Total error (m) | Image (pixel) |
|---|---|---|---|---|---|---|---|
| 1945 | 10 | 6 | 3.17 | 1.39 | 2.58 | 4.32 | 0.657 |
| 1954 | 9 | 7 | 2.72 | 1.59 | 2.01 | 3.74 | 0.873 |
| 1981 | 8 | 9 | 0.42 | 0.48 | 0.62 | 1.01 | 0.539 |
| 1986 | 9 | 5 | 1.37 | 1.37 | 1.73 | 2.60 | 0.521 |
| 1991 | 9 | 7 | 0.91 | 1.11 | 1.33 | 1.96 | 0.362 |
| 2003 | 10 | 5 | 0.99 | 1.41 | 1.13 | 2.06 | 0.392 |

providing a time series corrected for diffuse noise or trends. The data recorded on the landslide-prone area were analysed investigating the velocity of displacement along the LOS and reprojected along the slope (Notti et al. 2014). The combination of the acquired velocities by both ascending and descending orbits can decompose the detected motion along the LOS into horizontal and vertical components (Manzo et al. 2006; Notti et al. 2014). The component conversion is made by formulas that take into consideration the LOS directional cosines for the ascending and descending passes.

### Field surveys

After the main event in January 2003, several field surveys were performed by means of direct investigations and instrumental monitoring. The geology of the landslide-prone area was investigated by a field campaign and took advantage of several boreholes equipped by inclinometers.

Starting in 2010, several differential GPS measurement campaigns were conducted to monitor the remedial maintenance to intercept and drain surface waters by means of benchmarks and corner reflectors, which are currently partially lost and useless due to the continued displacement, vegetation and human activities. All campaigns were based on three stable points located outside the landslide.

Furthermore, two recent campaigns were conducted to highlight the geomorphological features to identify possible further changes. In 2014 and 2015, several scarps and counterslopes were detected and mapped.

### Results

#### 3D reconstruction of historical aerial photographs

The application of the SfM technique on sets of historical aerial photographs was useful to partially fill the temporal gap between
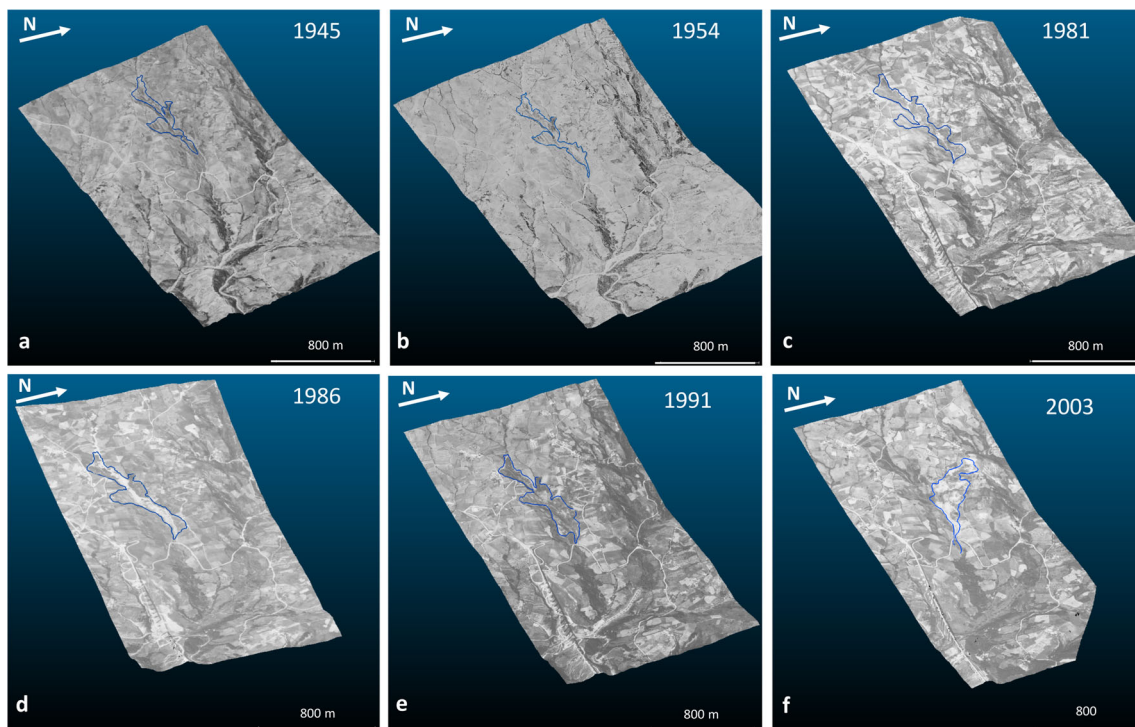


**Fig. 5** 3D reconstruction of the Colle Lapponi-Piano Ovetta landslide-prone area made by a set of historical aerial photographs that date back to 1945 (**a**), 1954 (**b**), 1981 (**c**), 1986 (**d**), 1991 (**e**) and 2003 (**f**). The landslide contour is plotted in blue

the beginning of the twentieth century and the main reactivation in 2003, with no information on the geomorphological evolution of the landslide. The procedure, with dedicated settings for historical photos, was applied to each scenario to extract the respective 3DPC and models. The results were individually analysed zooming and rotating the 3D model to better detect and map the contour of the landslide with respect to the classical stereoscopy by means of the Cloud Compare software. In addition, the resulting 3D reconstruction was integrated in the environmental GIS in order to obtain a better interpretation combined with the available ancillary data, e.g., Aspect and Slope. The first set of photographs refer to 1945 (Fig. 5a), in which an area affected by the landslide was visually recognized at the right flank of the basin damaging the access road to Piano Ovetta. It is difficult to confirm if the phenomenon was an activation or reactivation of an existing old mass movement because previous maps are not available. The contour map based on the analysis of the 3D reconstruction contains a visible area of approximately 0.86 km² that features displaced material with an average length and width of approximately 900 and 100 m, respectively.

The subsequent analysis included the set of photos from 1954 (Fig. 5b), in which no additional differences were recognized with respect to the previous set from 1945. In fact, the dimensions of the landslide are comparable to those of the previous reconstruction, and only small changes in the length, up to 1 km, are recognizable.

The flight conducted by the IGM over this territory was repeated in 1981 acquiring five additional photographs. After 25 years, the results are comparable to the previous analysis, with some small differences recognizable only on one side of the main body (Fig. 5c). Some lateral sliding, probably due to water erosion operating on the toe, is distinguishable. In fact, the length of the landslide is similar to that from the previous years. However, the width of the landslides increased due to some lateral slides that enlarged the area involved. An analogous boundary, with less evidence of lateral sliding, can be mapped on the 3D reconstruction of the CL-PO landslide-prone area in the 1986 reconstruction (Fig. 5d).

In the reconstruction of 1991 (Fig. 5e), remedial work conducted between 1986 and 1991 is recognizable (Fig. 6a). These man-made activities are visible as perpendicular white strips across the river along the width of the landslide (into Verrino creek). They consisted of concrete weirs built to avoid the continuous enlargement of the landslide due to span erosion and to control the amount of mobilized material run off. Currently, they are not visible inside the landslide due to the remobilization of material during the 2003 reactivation, but some of them were

recognizable in the widespread vegetation close to Verrino creek (Fig. 6b).

The 3D reconstruction made from the 2003 imagery shows the involvement of the left flank of the basin (Fig. 5f). Between January 23rd and 27th, an unusual increase in pore pressures caused by an intense rainfall of more than 200 mm in 72 h (Fig. 7a) occurred, triggering the complex deep-seated mass movement (Calcaterra et al. 2008) consisting of the reactivation of an old dormant landslide. The upper member of the Agnone Flysch was involved in a large roto-translational slide resulting in earth flow (Cruden and Varnes 1996), including an area of approximately 1.21 km² that was up to 1 km in length and had an average width of 200 m, which completely altered the local hydrographic network (Fig. 7b).

**DInSAR technique results**

The ERS1/2 PS data are very sparse for the period of 1992–2000 due to the spread of vegetation and the low presence of outcrops and structures (Fig. 8a). They are mainly localized on buildings and structures in the surrounding area of the landslide. The main movement is recognizable on the left flank (Fig. 8b) and on the structure of the current crown.

In March 2004 and between December 2004 and January 2005, several rainfall episodes affected the area again, causing two minor reactivations. The mobilized total volume of the whole landslide area was estimated at $3.5 \times 10^6$ m³ (Calcaterra et al. 2008), and it caused new damage to buildings and infrastructure. An additional advancement in the movement of the landslide toe was detected in June 2006 and between April 2006 and April 2007. Consequently, new mitigation measures were tracked into the body of the landslide, i.e. a new reshaping of the slope and 10 trench drains. These actions allowed the stabilization of the middle-lower region of the landslide body.

The ENVISAT PS data (2003–2010) are concentrated on the structure located on the crown. The ascending PS data show average velocities between − 3.0 and − 4.9 mm/year with a peak of − 7.0 mm/year, while the descending data are close to the stability range (Fig. 9a). The time series of the ENVISAT data, mainly in descending geometry, are noisy, but the trends of both orbits confirm continuous displacement (green line in Fig. 9b).

Furthermore, from 2012 to 2015, the COSMO-SkyMed data show displacement, although slow, demonstrating that the landslide movement is still active. The ascending PS data show a relatively constant velocity on buildings located in the current crown of the landslide, exhibiting important displacements with a peak of −



**Fig. 6** Location of the remedial work visible on the historical aerial reconstruction (**a**); details of the concrete weirs built along the tributary of the Verrino Creek (**b**)
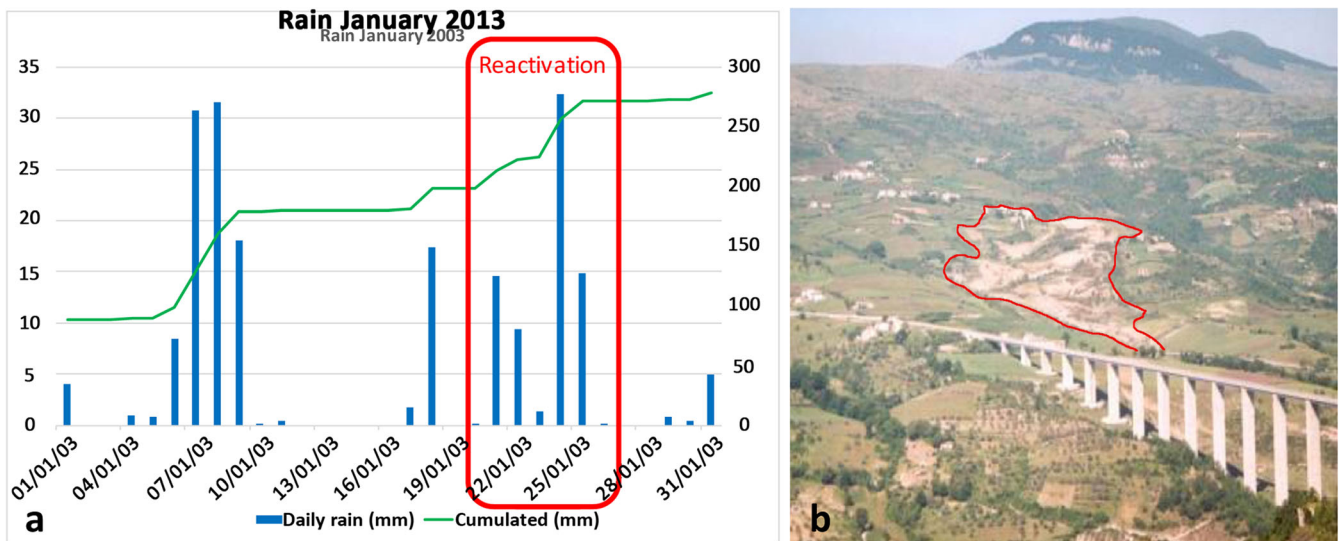
**Fig. 7** Daily (blue) and cumulative (green) rainfall (**a**); optical image of the study area (the landslide is delineated by a red line) (**b**)

11.6 mm/year. In descending geometry, despite very noisy data, the movement is confirmed with recorded velocities of + 7 mm/year moving toward the sensors (Fig. 10a). As shown in this figure, the location of several scarps corresponds to the buildings, thus confirming the retrogressive trend of the landslide. Moreover, these results have also been observed by the damage recorded on the buildings. Figure 10b shows a time series of the ascending PS data for construction on the crown of the landslide. It is interesting to note that the building located on the left flank of the boundary shows a displacement moving away from the crown (yellow circle in Fig. 10a). This is probably due to the fact that this sector is affected by a different mass movement, which induces displacements in the North-West direction.

### Field campaigns and in situ results

After the main reactivation, several in situ measurements and field campaigns were performed to monitor the evolution of the landslide. From 2006 to 2007, eight inclinometer measurements,

in addition to the "zero reading", were conducted showing important displacements at different depths, after which almost all the inclinometer casing tubes were broken (Fig. 11a). In the upper part of the landslide body, the inclinometer "S4" exhibits an important displacement with a sliding surface at approximately 25 m under the ground surface (Fig. 11b). The graph of the inclinometer "S5" reveals that the instrumentation was not locked on a stable bedrock, indicating only that the sliding surface is deeper than 25 m from the ground level (Fig. 11c). Using the in situ measurements, it was possible to trace the sliding surface (Fig. 11d) considering that the CL-PO landslide involves the upper members of the Agnone Flysch, dated as Lower Messinian (Vezzani et al. 2004).

The enlargement of the territory involved in the landslide by continued displacement is visually recognizable through optical photographs shot from the same point of view (Fig. 12a–c).

The enlargement of the landside area for the period of the GPS in situ measurement (2010–2016), combined with optical photographs
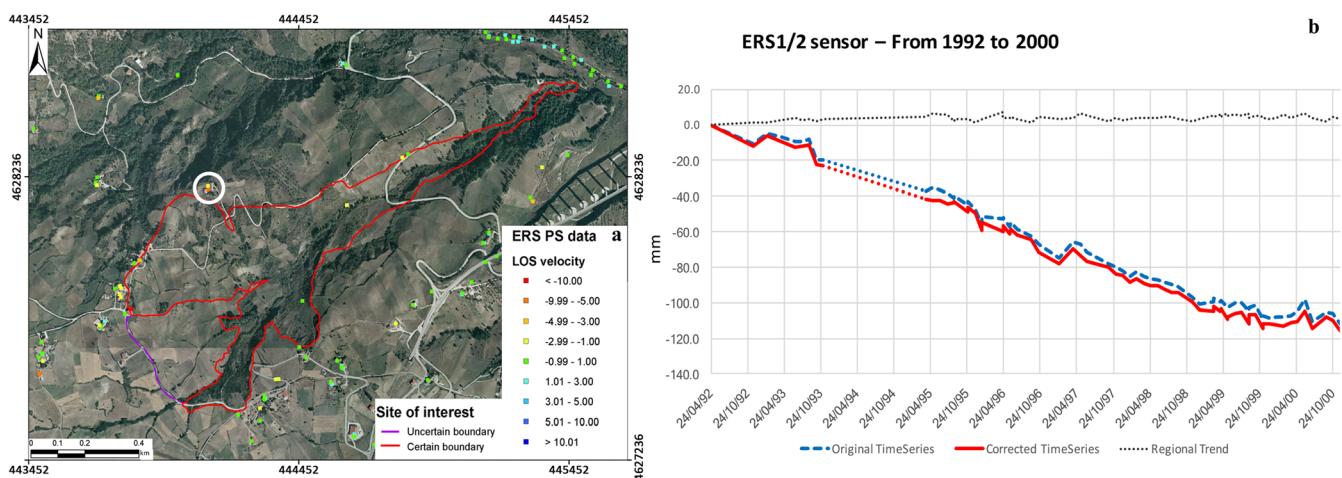


**Fig. 8** Distribution of ERS ascending data for the period of 1992–2000 (**a**); regional trend, original and corrected time series of the points in the white circle (**b**)
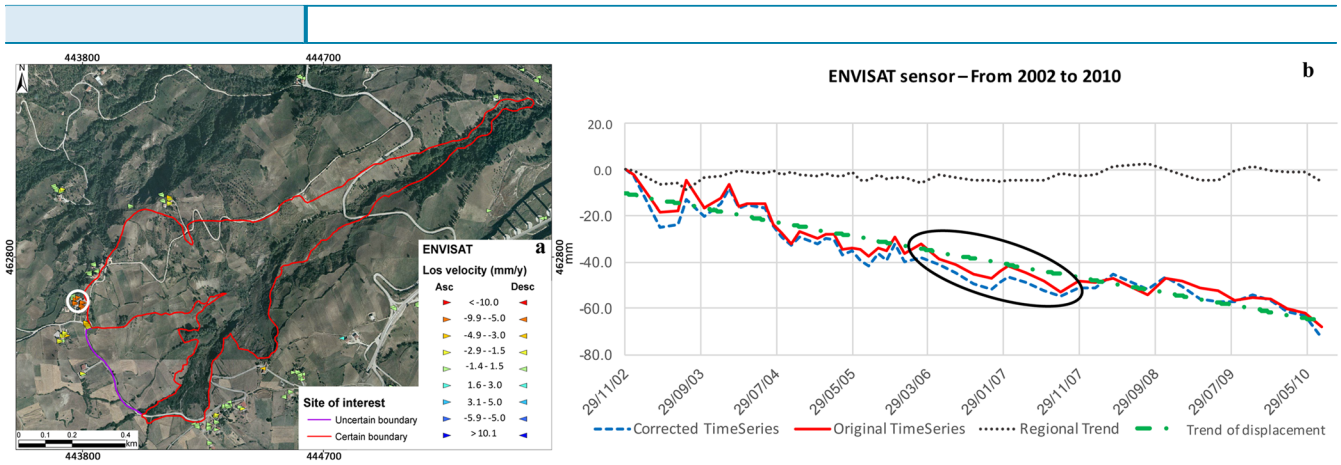
**Fig. 9** **a** PS distribution in the area of interest of the CL-PO landslide. **b** Regional trend and original and corrected time series of a PS located on the crown of the landslide. The black ellipsis highlights where the main reactivations occurred

and field surveys, was estimated to have approximately 350 m of advancement at the toe and approximately 270 m of retrogression at the head sector, reaching a total length up to 1500 m. The GPS field survey results in order to record the displacement measurements from 2010 to 2016 are visible in Fig. 13a. During the campaign conducted in November 2015 and July 2016, not all benchmarks were found because some of them were destroyed for building the drains or lost because of the continuous displacement affecting the slope. By means of the field surveys, it was possible to design a geomorphological map of the area influenced by the landslide and its surroundings by conducting several geomorphological field campaigns (Fig. 13a) where several old and recent scarp and counterslope shapes were noted.

In addition to the geomorphological shales, the area influenced by the landslide is currently covered by vegetation (Fig. 13b, c), suggesting a reduction in the movement over the last few years due to the remedial work.
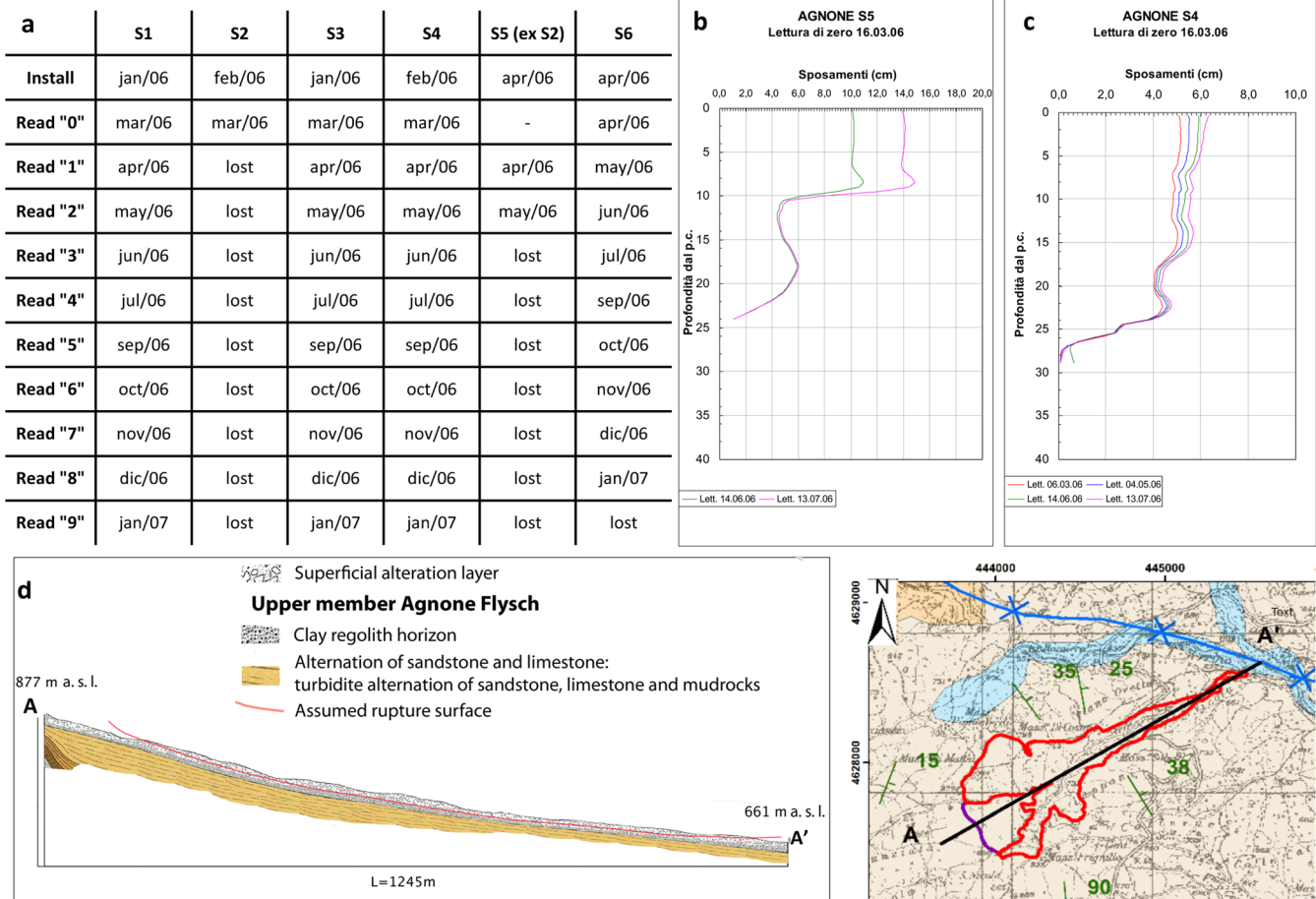
## Discussion

The multitechnique integration for multitemporal investigations enabled the analysis of one century of complex CL-PO mass movements. First, data were found in the literature from the

beginning of the twentieth century. Then, focus returned in 2003 when an important reactivation occurred. To investigate the evolution of landslide and erosional processes in the area, historical aerial photographs and InSAR techniques were utilized.

Historical photographs have already been applied to the DEM reconstruction using the SfM technique (Dewitte et al. 2008; Ishiguro et al. 2016) along with stereophotogrammetry. This data along with SfM-MVS has been applied for the diachronic reconstruction of geomorphological landscape evolution (Gomez et al. 2015), active volcanic areas (Gomez 2014; Ishiguro et al. 2016), glaciological monitoring (Kjeldsen et al. 2015; Midgley and Tonkin 2017) and erosion in river changes (Tonkin et al. 2016). Recently, different multitemporal landslide mapping and monitoring by means of the SfM approach was made, using the multi-sensor drone to capture the scene with RGB aerial images in high-resolution (e.g. Marek et al. 2015; Peternel et al. 2017; Rossi et al. 2018). For analysing the evolution of landslides, historical aerial images were already used, but without adopting the SfM approach (e.g. Casson et al. 2003; Guerriero et al. 2013). In this work, several previous applied approaches were merged to investigate as longest period as possible of the CL-PO
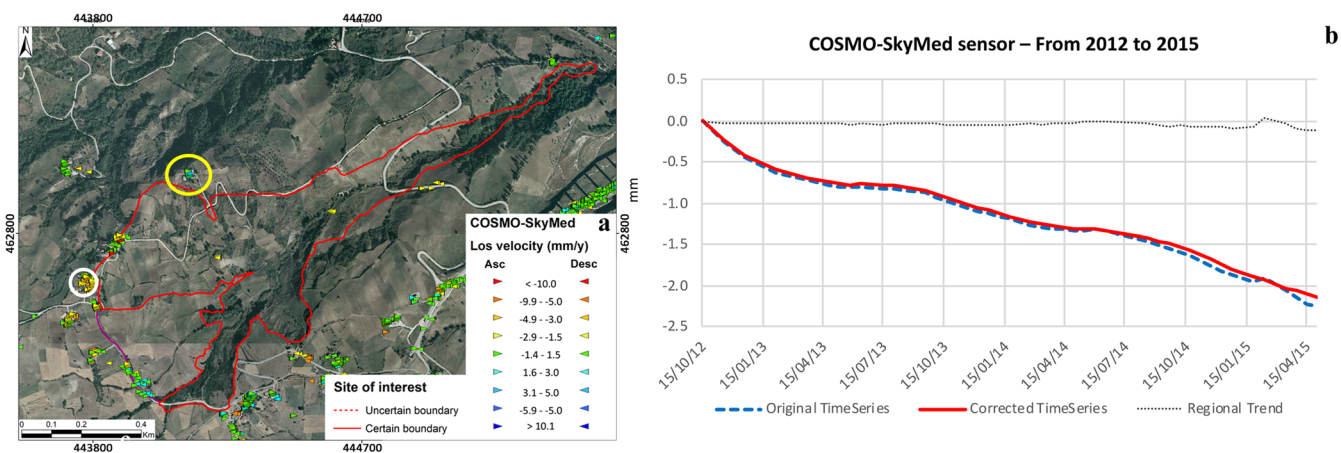


**Fig. 10** COSMO-SkyMed PS data in the area of interest of the CL-PO landslide (**a**). The yellow circle indicates a construction that shows an inversion of the velocity of displacement, while the white circle shows the location of the sample time series (**b**) corrected by the Notti et al. (2014) approach

| a | S1 | S2 | S3 | S4 | S5 (ex S2) | S6 |
|---|-----|-----|-----|-----|-----|-----|
| Install | jan/06 | feb/06 | jan/06 | feb/06 | apr/06 | apr/06 |
| Read "0" | mar/06 | mar/06 | mar/06 | mar/06 | - | apr/06 |
| Read "1" | apr/06 | lost | apr/06 | apr/06 | apr/06 | may/06 |
| Read "2" | may/06 | lost | may/06 | may/06 | may/06 | jun/06 |
| Read "3" | jun/06 | lost | jun/06 | jun/06 | lost | jul/06 |
| Read "4" | jul/06 | lost | jul/06 | jul/06 | lost | sep/06 |
| Read "5" | sep/06 | lost | sep/06 | sep/06 | lost | oct/06 |
| Read "6" | oct/06 | lost | oct/06 | oct/06 | lost | nov/06 |
| Read "7" | nov/06 | lost | nov/06 | nov/06 | lost | dic/06 |
| Read "8" | dic/06 | lost | dic/06 | dic/06 | lost | jan/07 |
| Read "9" | jan/07 | lost | jan/07 | jan/07 | lost | lost |

**Fig. 11** Summary of the investigation conducted with the inclinometers (**a**), with examples of S5 (**b**) and S4 (**c**). Section of the CL-PO landslide update with the assumed rupture surface traced with the info derived by the in situ measurements (**d**)

landslide evolution, taking advantage from historical aerial images not widely exploited by SfM approach despite its great potential.

This paper presents the multitemporal analysis applied to six sets of historical photographs from 1945 to 2003, which enabled the recognition of the geomorphological evolution of the CL-PO landslide over approximately 60 years. The SfM technique, adapting the standard digital method to non-digital historical aerial photographs, enabled the reconstruction of precise digital models to analyse the environmental evolution of the area of interest. Although difficulties arose during the processing due to the age and the state of preservation of the printed and scanned photos, along with their resolution, 3D reconstructions were developed for each set of photographs. Furthermore, stable points recognizable in every scenario for good georeferencing were difficult to find due to the resolution of the photographs. The main differences between the 3D model from 1954 to 2003 were identified in the medium and upper portion of the mass movement where the morphology was strongly affected by the complex landslide that even now results in a continuously slow evolution. Less relevant



**Fig. 12** Optical photographs in 2004 (**a**), 2005 (**b**) and 2007 (**c**)
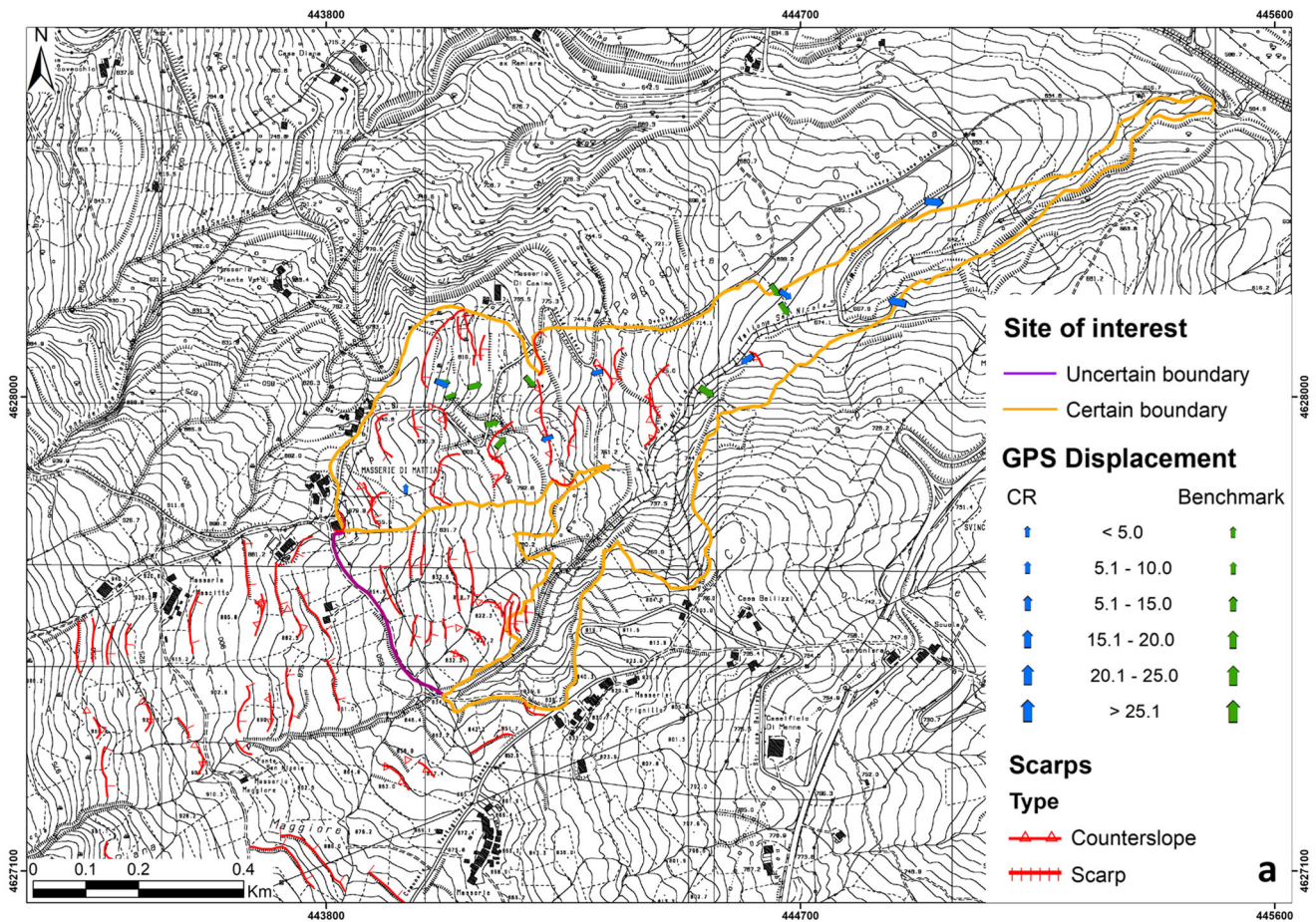
**Fig. 13** Geomorphological maps of the landslide-prone CL-PO area and GPS displacements recorded from 2010 to 2016 (**a**). Optical photographs of the landslide on November 2015 (**b**) and July 2016 (**c**)

modifications with enlargements were also recognized on the lateral sides and the toe of the landslide, probably due to the lateral sliding and material transported by the tributary of the Verrino Creek.

Since 1992, ERS, ENVISAT and COSMO-SkyMed PS data record displacements with high precision where reflectors, i.e. outcrops or infrastructure, were combined with optical photos

allowing us to see important changes, including the vegetated areas. Three matters have to be addressed: (a) the PS uphill with respect to the crown of the landslide show, even if with small values, velocities indicating movement in this portion of the basin; (b) COSMO-SkyMed data show continued slow displacement, suggesting that the adopted measurements after the main reactivation were not sufficient to completely stop the

advancement of the mass movement; (c) the COSMO-SkyMed PS data recorded on two buildings that were strongly damaged located on the left flank of the landslide show a displacement moving through the sensor, while in the ERS 1/2 and ENVISAT monitoring period, they exhibited movements away from the satellites. The change in movement direction can be ascribed to the involvement of this portion of the landslide by a mass movement affecting the closest basin, which is increasing in dimension. Some opening fractures recognizable between two portions of the building support this hypothesis. It confirms the relevant impacts of landslide and erosional processes affecting the whole territory of the Agnone municipality and the Molise region.

To validate the remote sensing data interpretation, combined with the inclinometers and GPS measurement campaigns, several field and geomorphological surveys were recorded in the landslide area. Field campaigns were conducted to investigate the geology of the landslide, to validate the velocity of displacement, and to identify the depth of the sliding surface. Recent optical photographs show gibbous shapes, as well as direct and indirect field measurements conducted specifically to identify the geomorphological evidence, confirming the continued displacement and topographical evolution of the upper part of the landslide and the area uphill from the crown. Continued displacements and reactivations of a portion or of the total landslide suggested that the designed countermeasures, i.e. drainages and reshaping, are inadequate to stop the displacement. The countermeasures helped to reduce the velocity of displacement and to stabilize and increase drainage in the middle-lower region of the landslide but not to stabilize the entire region involved in the 2003 reactivation.

The continue displacement of the landslide is confirmed also by the couple of CR and benchmarks placed out of the boundary of the mass movement. They exhibit a steady displacement due to the continuous enlargement of the influenced area and suggest, according to the analysis of the direct and indirect measurements that the geomorphological evolution of the area could continue in the future. The past development of the landslide, the continuous recorded displacement by PS data and the identified geomorphological shapes recognized in the uphill area with respect to the body of the landslide are relevant indicators. Furthermore, the recognized cracks in the asphalt and weak damage on infrastructure made to stabilize the upper region of the right flank, e.g. some gabions, support the hypothesis that the area could be susceptible to another reactivation.

The application of the SfM on historical aerial images, in addition to the combination of multisource data, can strongly improve the knowledge on the landslide-prone areas and of the possible consequences in case of landslide occurrence, being very useful for avoiding further recurrences.

### Conclusions

One century of the complex CL-PO mass movement was investigated by integrating highly heterogeneous multisource data, e.g. literature data, historical aerial photographs and InSAR products.

A literature analysis was conducted to collect information about the landslide occurring at the beginning of the twentieth century. Subsequently, six sets of historical aerial photographs from 1945 to 2003 were analysed by means of the SfM approach in order to extract the geomorphological evolution of the landslide-prone area by developing a 3D model of each scenario. The combination and analysis of the 3D reconstructions enable the recognition of the oldest landslide affecting the right side of the catchment, the evolution over time and the subsequent event that occurred in 2003 involving the left side. In 1945, a landslide on the right flank of the basin had already occurred. From 1945 to 1991, no important landslide evolution was identified, except small lateral sliding with material tumbling at the foot of the landslide body. The benefits of the adopted measurement for the right flank, recognizable by the 3D reconstructions between 1986 and 1991, e.g. gabions and weirs in the river, were confirmed in 2003 when a reactivation landslide involved an extended area on the left flank of the basin, which damaged several buildings and infrastructure. Then, from 1992 to 2015, PS data of ERS and ENVISAT, C-band satellite, and COSMO-SkyMed, X-band constellation, were investigated to monitor the recent evolution. ERS data exhibit a few stable PS close to the right boundary of the landslide, showing velocities of approximately − 3.5 mm/year along the LOS of the satellite on structures at the left flank. The ENVISAT data show important velocity measurements, even if they are noisy, on the buildings at the upstream portion of the basin, confirmed by COSMO-SkyMed data showing continued slow displacement. All the information recorded by the remote sensing technique were integrated with field investigations and ancillary data derived from geotechnical and geomorphological surveys, GPS campaigns, and inclinometer and pluviometer measurements. The analysis of the last few decades identified the portion of the landslide mainly affected by displacement and enabled the monitoring of effects from the remedial work after the main reactivation in 2003. The recent data demonstrated that the movements were drastically reduced, if not completely halted.

The study area has drawn the attention of the scientific community due to the 2003 reactivation that damaged buildings and infrastructure, with possible social and economic consequences. The extent of the damage forced the local administrator to propose restrictive measurements for some edifices. In this work, a complete investigation of the past and present deformational scenarios allowed the planning of potential additional mitigation and prevention strategies to avoid further possible reactivations. In the future, the continued analysis by InSAR techniques, e.g. high-resolution COSMO-SkyMed images and field measurements, could be useful to monitor the evolution of the landslide that could involve other structures and infrastructure located upstream.

DIFSAR data from the Extraordinary Plan of Environmental Remote Sensing (EPRS-E) were made available through the *Portale Cartografico Nazionale* of the Italian Ministry of Environment, Territory and Sea (MATTM) due to a specific agreement. The authors would like to thank the editor and the three anonymous reviewers for their valuable comments and suggestions to improve the quality of the paper.

## References

Abellán A, Jaboyedoff M, Oppikofer T, Vilaplana J (2009) Detection of millimetric deformation using a terrestrial laser scanner: experiment and application to a rockfall event. Nat Hazards Earth Syst Sci 9:365–372

Agisoft (2016) Agisoft PhotoScan user manual professional edition, version 1.2. Agisoft LLC, St Petersburg

Almagià R (1910) Studi geografici sulle frane in Italia. Vol. II. L'Apennino centrale e meridionale. Conclusioni generali. Società Geografica Italiana (IS)

Blanco-Sanchez P, Mallorquí JJ, Duque S, Monells D (2008) The coherent pixels technique (CPT): an advanced DInSAR technique for nonlinear deformation monitoring. Pure Appl Geophys 165:1167–1193

Calcaterra D, Di Martire D, Ramondini M, Calò F, Parise M (2008) Geotechnical analysis of a complex slope movement in sedimentary successions of the southern Apennines (Molise, Italy). Landslides Eng Slopes:299–305

Carrara A, Crosta G, Frattini P (2003) Geomorphological and historical data in assessing landslide hazard. Earth Surf Process Landf 28:1125–1142

Casson B, Delacourt C, Baratoux D, Allemand P (2003) Seventeen years of the "La Clapière" landslide evolution analysed from ortho-rectified aerial photographs. Eng Geol 68:123–139. https://doi.org/10.1016/S0013-7952(02)00201-6

Cigna F, Del Ventisette C, Liguori V, Casagli N (2011) Advanced radar-interpretation of InSAR time series for mapping and characterization of geological processes. Nat Hazards Earth Syst Sci 11:865–881

Confuorto P, Di Martire D, Centolanza G, Iglesias R, Mallorqui JJ, Novellino A, Plank S, Ramondini M, Thuro K, Calcaterra D (2017) Post-failure evolution analysis of a rainfall-triggered landslide by multi-temporal interferometry SAR approaches integrated with geotechnical analysis. Remote Sens Environ 188:51–72

Costantini M, Falco S, Malvarosa F, Minati F (2008) A new method for identification and analysis of persistent scatterers in series of SAR images. In Geoscience and Remote Sensing Symposium, 2008. IGARSS 2008. IEEE international (Vol. 2, pp II-449). IEEE

Cotecchia V, Melidoro G (1974) Some principal geological aspects of the landslides of southern Italy. Bull Int Assoc Eng Geol-Bulletin de l'Association Internationale de Géologie de l'Ingénieur 9:23–32

Crozier MJ (2010) Deciphering the effect of climate change on landslide activity: a review. Geomorphology 124:260–267

Cruden DM, Varnes DJ (1996) Landslides: investigation and mitigation. Chapter 3- Landslide types and processes. Transportation research board special report

Dekker R (2005) SAR change detection techniques and applications. EARSeL, Munster

Del Soldato M, Di Martire D, Tomas R (2016a) Comparison of different approaches for landslide-induced damage assessment: the case study of Agnone (southern Italy). Rendiconti Online Società Geologica Italiana 41:139–142

Del Soldato M, Riquelme A, Tomàs R, De Vita P, Moretti S (2016b) Geomorphological investigation based on 3D historical reconstruction. In Geosciences on a changing planet: learning from the past, exploring the future. Società Geologica Italiana, Roma

Del Soldato M, Bianchini S, Calcaterra D, De Vita P, Martire DD, Tómas R, Casagli N (2017) A new approach for landslide-induced damage assessment. Geomat Nat Haz Risk:1–14

Dewitte O, Jasselette J-C, Cornet Y, Van Den Eeckhaut M, Collignon A, Poesen J, Demoulin A (2008) Tracking landslide displacements by multi-temporal DTMs: a combined aerial stereophotogrammetric and LIDAR approach in western Belgium. Eng Geol 99(1):11–22. https://doi.org/10.1016/j.enggeo.2008.02.006

Di Maio C, Vassallo R, Vallario M, Pascale S, Sdao F (2010) Structure and kinematics of a landslide in a complex clayey formation of the Italian southern Apennines. Eng Geol 116:311–322

Doneus M, Verhoeven G, Fera M, Briese C, Kucera M, Neubauer W (2011) From deposit to point cloud–a study of low-cost computer vision approaches for the straightforward documentation of archaeological excavations. Geoinformat FCE CTU 6:81–88

Eltner A, Kaiser A, Castillo C, Rock G, Neugirg F, Abellán A (2016) Image-based surface reconstruction in geomorphometry–merits, limits and developments. Earth Surf Dyn 4:359–389

Esu F (1977) Behaviour of slopes in structurally complex formations. In: Proceedings of the international symposium on the geotechnics of structurally complex formations, pp 292–304

Farina P, Colombo D, Fumagalli A, Marks F, Moretti S (2006) Permanent scatterers for landslide investigations: outcomes from the ESA-SLAM project. Eng Geol 88:200–217

Ferretti A, Prati C, Rocca F (2000) Nonlinear subsidence rate estimation using permanent scatterers in differential SAR interferometry. IEEE Trans Geosci Remote Sens 38:2202–2212

Ferretti A, Prati C, Rocca F (2001) Permanent scatterers in SAR interferometry. IEEE Trans Geosci Remote Sens 39:8–20

Filocamo F, Rosskopf CM, Amato V, Cesarano M, Di Paola G (2015) The integrated exploitation of the geological heritage: a proposal of geotourist itineraries in the Alto Molise area (Italy). Rend Online Soc Geol Ital 33:44–47. https://doi.org/10.3301/ROL.2015.11

Fisher RB, Breckon TP, Dawson-Howe K, Fitzgibbon A, Robertson C, Trucco E, Williams CK (2013) Dictionary of computer vision and image processing. John Wiley & Sons

Furukawa Y, Ponce J (2010) Accurate, dense, and robust multiview stereopsis. IEEE Trans Pattern Anal Mach Intell 32:1362–1376

Giordan D, Allasia P, Manconi A, Baldo M, Santangelo M, Cardinali M, Corazza A, Albanese V, Lollino G, Guzzetti F (2013) Morphological and kinematic evolution of a large earthflow: the Montaguto landslide, southern Italy. Geomorphology 187:61–79

Gomez C (2014) Digital photogrammetry and GIS-based analysis of the bio-geomorphological evolution of Sakurajima volcano, diachronic analysis from 1947 to 2006. J Volcanol Geotherm Res 280:1–13. https://doi.org/10.1016/j.jvolgeores.2014.04.015

Gomez C, Hayakawa Y, Obanawa H (2015) A study of Japanese landscapes using structure from motion derived DSMs and DEMs based on historical aerial photographs: new opportunities for vegetation monitoring and diachronic geomorphology. Geomorphology 242:11–20

Guerriero L, Revellino P, Coe JA, Focareta M, Grelle G, Albanese V, Corazza A, Guadagno FM (2013) Multi-temporal maps of the Montaguto earth flow in southern Italy from 1954 to 2010. J Maps 9(1):135–145

Guida D, Iaccarino G (1991) Fasi evolutive delle frane di tipo colata nell'alta valle del F. Basento (Potenza). Studi trentini di scienze naturali. Acta geologica 68:127–152

Guzzetti F, Cardinali M, Reichenbach P (1994) The AVI project: a bibliographical and archive inventory of landslides and floods in Italy. Environ Manag 18:623–633

Hapke C (2005) Estimation of regional material yield from coastal landslides based on historical digital terrain modelling. Earth Surf Process Landf 30:679–697

Hartley R, Zisserman A (2003) Multiple view geometry in computer vision. Cambridge University Press

Herrera G, Mateos RM, García-Davalillo JC, Grandjean G, Poyiadji E, Maftei R, Filipciuc TC, Auflič MJ, Jež J, Podolszki L, Trigila A, Iadanza C, Raetzo H, Kociu A, Przyłucka M, Kułak M, Sheehy M, Pellicer XM, McKeown C, Ryan G, Kopačková V, Frei M, Kuhn D, Hermanns RL, Koulermou N, Smith CA, Engdahl M, Buxó P, Gonzalez M, Dashwood C, Reeves H, Cigna F, Liščák P, Pauditš P, Mikulénas V, Demir V, Raha M, Quental L, Sandić C, Fusi B, Jensen OA (2018) Landslide databases in the geological surveys of Europe. Landslides:1–21

Hooper A, Bekaert D, Spaans K, Arıkan M (2012) Recent advances in SAR interferometry time series analysis for measuring crustal deformation. Tectonophysics 514:1–13

Iglesias R, Monells D, López-Martínez C, Mallorqui JJ, Fabregas X, Aguasca A (2015) Polarimetric optimization of temporal sublook coherence for DInSAR applications. IEEE Geosci Remote Sens Lett 12:87–91

Ishiguro S, Yamano H, Oguma H (2016) Evaluation of DSMs generated from multi-temporal aerial photographs using emerging structure from motion–multi-view stereo technology. Geomorphology 268:64–71

James MR, Robson S (2014) Mitigating systematic error in topographic models derived from UAV and ground-based image networks. Earth Surf Process Landf 39:1413–1420

Kjekstad O, Highland L (2009) Economic and social impacts of landslides

Kjeldsen KK, Korsgaard NJ, Bjørk AA, Khan SA, Box JE, Funder S, Larsen NK, Bamber JL, Colgan W, van den Broeke M, Siggaard-Andersen ML, Nuth C, Schomacker A, Andresen CS, Willerslev E, Kjær KH (2015) Spatial and temporal distribution of mass

loss from the Greenland ice sheet since AD 1900. Nature 528(7582):396–400. https://doi.org/10.1038/nature16183

Korup O, Densmore AL, Schlunegger F (2010) The role of landslides in mountain range evolution. Geomorphology 120:77–90

Lu D, Mausel P, Brondizio E, Moran E (2004) Change detection techniques. Int J Remote Sens 25:2365–2401

Lucieer A, de Jong S, Turner D (2013) Mapping landslide displacements using structure from motion (SfM) and image correlation of multi-temporal UAV photography. Prog Phys Geogr 0309133313515293

Manzo M, Ricciardi GM, Casu F, Ventura G, Zeni G, Borgström S, Berardino P, Del Gaudio C, Lanaria R (2006) Surface deformation analysis in the Ischia Island (Italy) based on spaceborne radar interferometry. J Volcanol Geotherm Res 151:399–416

Marchetti M (2016) Consumo di suolo, dinamiche territoriali e servizi ecosistemici. Edizione

Marek L, Miřijovský J, Tuček P (2015) Monitoring of the shallow landslide using UAV photogrammetry and geodetic measurements. In: Lollino G. et al. (eds) Engineering geology for society and territory - volume 2. Springer

Massonnet D, Feigl KL (1998) Radar interferometry and its application to changes in the Earth's surface. Rev Geophys 36:441–500

Meisina C, Zucca F, Notti D, Colombo A, Cucchi A, Savio G, Giannico C, Bianchi M (2008) Geological interpretation of PSInSAR data at regional scale. Sensors 8:7469–7492

Midgley NG, Tonkin TN (2017) Reconstruction of former glacier surface topography from archive oblique aerial images. Geomorphology 282:18–26. https://doi.org/10.1016/j.geomorph.2017.01.008

Mora O, Mallorqui JJ, Broquetas A (2003) Linear and nonlinear terrain deformation maps from a reduced set of interferometric SAR images. IEEE Trans Geosci Remote Sens 41:2243–2253

Notti D, Herrera G, Bianchini S, Meisina C, García-Davalillo JC, Zucca F (2014) A methodology for improving landslide PSI data analysis. Int J Remote Sens 35:2186–2214. https://doi.org/10.1080/01431161.2014.889864

Notti D, Fabiano C, Cigna F, Manunta M, Herrera G, Berti M, Meisina C, Tapete D, Zucca F (2015) A user-oriented methodology for DInSAR time series analysis and interpretation: landslides and subsidence case studies. Pure Appl Geophys 172:3081–3105

Peternel T, Kumelj S, Ostir K, Komac M (2017) Monitoring the Potoška planina landslide (NW Slovenia) using UAV photogrammetry and tachymetric measurements. Landslides 14:395–406

Riquelme AJ, Abellán A, Tomás R, Jaboyedoff M (2014) A new approach for semi-automatic rock mass joints recognition from 3D point clouds. Comput Geosci 68:38–52

Rossi G, Tanteri L, Tofani V, Vannocci P, Moretti S, Casagli N (2018) Multitemporal UAV surveys for landslide mapping and characterization. Landslides:1–8

Rosskopf C, Aucelli P (2007) Analisi del dissesto da frana in Molise

Salvati P, Rossi M, Bianchi C, Guzzetti F (2015) Landslide risk to the population of Italy and its geographical and temporal variations. Extreme Events Observ Model Econ 214:177

Schuster RL, Highland L (2001) Socioeconomic and environmental impacts of landslides in the western hemisphere. US Department of the Interior, US Geological Survey

Snavely N, Seitz SM, Szeliski R (2008) Modeling the world from internet photo collections. Int J Comput Vis 80:189–210

Solari L, Raspini F, Del Soldato M, Bianchini S, Ciampalini A, Ferrigno F, Tucci S, Casagli N (2018) Satellite radar data for back-analyzing a landslide event: the Ponzano (Central Italy) case study. Landslides 15:1–10. https://doi.org/10.1007/s10346-018-0952-x

Sturzenegger M, Stead D, Elmo D (2011) Terrestrial remote sensing-based estimation of mean trace length, trace intensity and block size/shape. Eng Geol 119:96–111

Szeliski R (2010) Computer vision: algorithms and applications. Springer Science & Business Media

Tonkin TN, Midgley NG, Cook SJ, Graham DJ (2016) Ice-cored moraine degradation mapped and quantified using an unmanned aerial vehicle: a case study from a polythermal glacier in Svalbard. Geomorphology 258:1–10. https://doi.org/10.1016/j.geomorph.2015.12.019

Turner D, Lucieer A, Watson C (2012) An automated technique for generating georectified mosaics from ultra-high resolution unmanned aerial vehicle (UAV) imagery, based on structure from motion (SfM) point clouds. Remote Sens 4:1392–1410

Ullman S (1979) The interpretation of visual motion. Massachusetts Inst of Technology Pr

Van Westen CJ, Lulie Getahun F (2003) Analyzing the evolution of the Tessina landslide using aerial photographs and digital elevation models. Geomorphology 54:77–89. https://doi.org/10.1016/S0169-555X(03)00057-6

Verhoeven G (2011) Taking computer vision aloft–archaeological three-dimensional reconstructions from aerial photographs with photoscan. Archaeol Prospect 18:67–73

Verhoeven G, Taelman D, Vermeulen F (2012) Computer vision-based orthophoto mapping of complex archaeological sites: the ancient quarry of Pitaranha (Portugal-Spain). Archaeometry 54:1114–1129

Vezzani L, Ghisetti F, Festa A, Follador U (2004) Carta geologica del Molise. SELCA

Westoby M, Brasington J, Glasser N, Hambrey M, Reynolds J (2012) 'Structure-from-Motion' photogrammetry: a low-cost, effective tool for geoscience applications. Geomorphology 179:300–314

White RG (1991) Change detection in SAR imagery. Int J Remote Sens 12:339–360

**M. Del Soldato** (✉) · **S. Bianchini** · **S. Moretti**
Department of Earth Sciences,
University of Firenze,
Via La Pira 4, 50121, Florence, Italy
Email: matteo.delsoldato@unifi.it

**M. Del Soldato** · **D. Di Martire** · **P. De Vita** · **D. Calcaterra**
Department of Earth Sciences, Environment and Resources,
Federico II University of Napoli,
Complesso Universitario di Monte Sant'Angelo, Napoli, Italy

**A. Riquelme** · **R. Tomàs**
Departamento de Ingeniería Civil, Escuela Politécnica Superior,
Universidad de Alicante,
P.O. Box 99E-03080, Alicante, Spain